Nanoscale characterization of plasma functionalized graphitic flakes using tip-enhanced Raman spectroscopy

Naresh Kumar,[1] Sofia Marchesini,[1] Thomas Howe,[2] Lee Edwards,[2] Barry Brennan,[1] and Andrew J. Pollard[1,a)]

AFFILIATIONS

[1] National Physical Laboratory, Hampton Road, Teddington TW11 0LW, United Kingdom
[2]Haydale Limited, Clos Fferws, Parc Hendre, Ammanford SA18 3BL, United Kingdom

Note: This paper is part of the JCP Special Topic on Spectroscopy and Microscopy of Plasmonic Systems.
[a)] Author to whom correspondence should be addressed: andrew.pollard@npl.co.uk

ABSTRACT

The chemical functionalization of graphene nanomaterials allows for the enhancement of their properties for novel functional applications. However, a better understanding of the functionalization process by determining the amount and location of functional groups within individual graphene nanoplatelets remains challenging. In this work, we demonstrate the capability of tip-enhanced Raman spectroscopy (TERS) to investigate the degree and spatial variability of the appearance of disorder in graphitic nanomaterials on the nanoscale with three different levels of nitrogen functionalization. TERS results are in excellent agreement with those of confocal Raman spectroscopy and chemical analysis, determined using x-ray photoelectron spectroscopy and time-of-flight secondary ion mass spectrometry, of the functionalized materials. This work paves the way for a better understanding of the functionalization of graphene and graphitic nanomaterials at the nano-scale, micro-scale, and macro-scale and the relationship between the techniques and how they relate to the changes in material properties of industrial importance.

I. INTRODUCTION

The chemical functionalization of graphene and graphitic nanomaterials is a powerful method to improve their dispersion characteristics and enhance material properties for applications such as polymer nanocomposites,[1] super-capacitor devices,[2] drug delivery systems,[3] memory devices,[4] solar cells,[5] and biosensors.[6,7] However, the characterization of chemical and structural changes in the functionalized materials at the nanoscale, introduced through the attachment of chemical groups, requires specialist techniques. Furthermore, determining the degree and location of the functional groups on the surface of individual graphitic flakes will be beneficial for optimizing material properties for desired applications, as the addition of chemical species can, for example, affect the dispersion of the material in solvents and resins as well as the mechanical strength of the graphene material itself.[8,9] However, this remains challenging, and currently, there is a lack of reliable analytical techniques that can distinguish between the level, location, or structure of functionalization at the level of single flakes or particles.

Over the last two decades, tip-enhanced Raman spectroscopy (TERS) has emerged as a powerful nanoanalytical tool for non-destructive molecular imaging at nanometer length-scales in the ambient environment.[10-14] TERS works on the principle of localized surface plasmon resonance in which a highly intense and localized electromagnetic field is created at the apex of a metallic probe placed in the focal spot of an excitation laser. Raman signals from molecules located in this "near-field" are enhanced by several orders of magnitude, which pushes the spatial resolution of molecular imaging far beyond the diffraction limit.[15] TERS has been successfully used for nanoscale chemical characterization in a wide range of research areas including heterogeneous catalysis,[16-18] organic

photovoltaic devices,[19,20] biological cells,[21,22] solid-liquid interfaces,[23] 1D materials such as single-wall carbon nanotubes,[24-27] and 2D materials including single-layer graphene[28-32] and MoS_2.[33-35] However, most of the TERS research to date has been restricted to model test systems, and application to real-life samples, especially of direct industrial relevance, has been very limited.

In this work, we extend the application of TERS to nanoscale characterization of commercially available, plasma-functionalized graphitic nanomaterials and demonstrate that in addition to model systems, TERS is capable of providing significant novel insights into real-world samples. TERS imaging of graphitic nanomaterials with three different levels of nitrogen functionalization is performed to determine the level and spatial distribution of chemical groups on individual graphitic flakes. Furthermore, in combination with confocal Raman spectroscopy, x-ray photoelectron spectroscopy (XPS), and time-of-flight secondary ion mass spectrometry (ToF-SIMS) measurements, our results show that TERS has the sensitivity to determine differences in the degree of chemical functionalization and provide spatially resolved information about the location of functionalization, which cannot be obtained non-destructively using existing analytical techniques under ambient conditions.

II. RESULTS AND DISCUSSION

Figure 1(a) shows a schematic diagram of the transmission-mode TERS system used in this work for nanoscale chemical imaging of flakes from a powder containing graphene nanoplatelets that has been plasma functionalized. This TERS system has previously provided a spatial resolution of 14 nm-51 nm in Raman imaging of a range of different samples including single-layer graphene[28,30] and MoS_2,[34] biological cells,[21] catalyst materials,[16] and organic photovoltaic devices.[19] Figures 1(b) and 1(c) show representative atomic force microscopy (AFM) topography and scanning electron microscopy (SEM) images of two samples, respectively, revealing graphitic materials. A high degree of heterogeneity was observed in the lateral size and thickness of graphitic flakes in the measured samples. For example, the thickness of the flakes measured from the sample depicted in Fig. 1(b) varied from 7 nm to 48 nm.

Figure 1(d) shows a confocal Raman spectrum of an unfunctionalized graphitic flake. In the Raman spectrum of graphene and graphitic materials, the D peak arises from the A_{1g} vibrational mode but is only visible in the vicinity of a structure-symmetry breaking feature such as vacancies, sp^3 bonding, or flake edges, whereas the G peak arises from the in-plane E_{2g} mode, which is common to all sp^2 carbon systems.[36-39] Therefore, the ratio of the intensity of the D peak (I_D) to that of the G peak (I_G), I_D/I_G, is an indicator of the level of disorder in graphene and graphitic materials.[40,41] A D peak was observed in the Raman spectrum together with the expected G and 2D peaks indicating disorder in the unfunctionalized graphitic material, which is usually expected to be associated with the edges of the graphitic flakes that have a lateral size comparable to or smaller than the probe size of confocal Raman spectroscopy.[42-44]

TERS and corresponding AFM images of an unfunctionalized graphitic flake are presented in Fig. 2. An AFM image showing the morphology of multiple graphitic particles is shown in Fig. 2(a), while Figs. 2(b) and 2(c) present TERS images of D and G peak intensities, respectively, of the single flake marked by the white box in Fig. 2(a). The lateral resolution of the TERS image in Fig. 2(b) is estimated to be 34 ± 9 nm, determined from the FWHM from the line profile in Fig. S1, but this value may be limited by the variations in the material itself. Similar to the far-field Raman spectrum shown in Fig. 1(d), a clear D peak was observed in all TERS spectra. In order to analyze the spatial variation of the lattice disorder in more detail, average TERS spectra measured in the central region of the flake and four different areas close to the edge region are shown in Fig. 2(d). In these spectra, D and G peaks were fitted using Lorentzian curves after linear background subtraction, and the intensity of the fitted

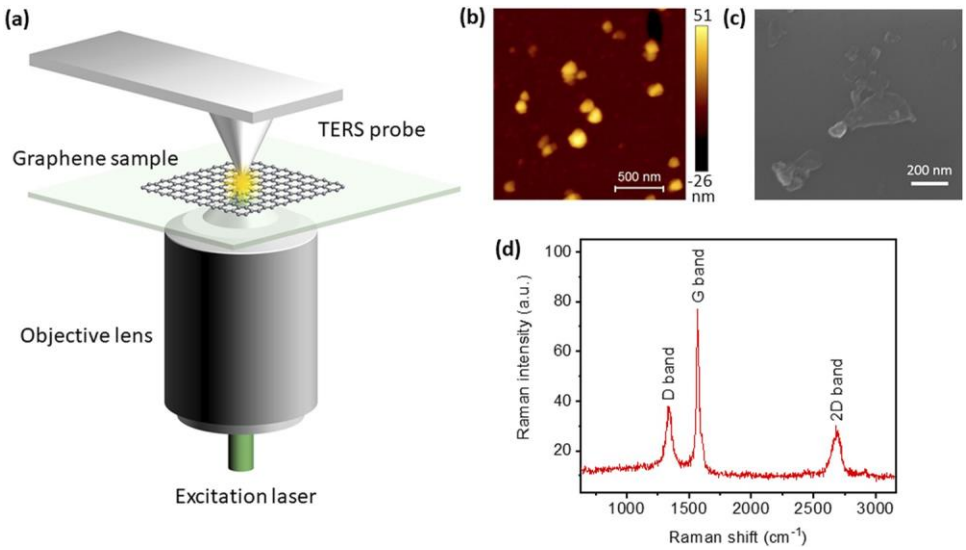

FIG. 1. (a) Schematic diagram of the transmission mode TERS setup used in this study. (b) AFM image of unfunctionalized graphitic flakes dispersed and deposited on a glass substrate. The dark region in the top right corner represents a surface feature that is typically observed for this type of substrate. (c) SEM image of nitrogen-functionalized graphitic flakes on a Si substrate. (d) Confocal Raman spectrum of an individual unfunctionalized graphitic flake showing D, G, and 2D peaks. Integration time: 10 s.

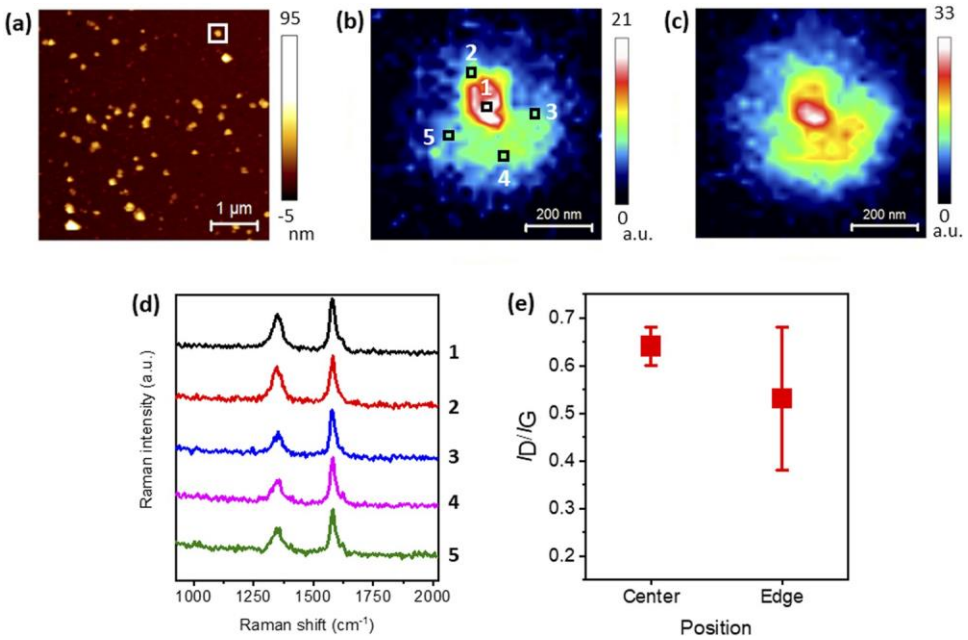

FIG. 2. (a) AFM topography image of unfunctionalized graphitic flakes dispersed on a glass substrate. TERS images of the (b) D peak and (c) G peak intensities of the graphitic flake marked in (a). Integration time: 1 s. Step size: 23 nm. (d) Plot of average TERS spectra measured in the central and edge regions of the flake marked in (b). Each spectrum represents an average of four spectra from adjacent pixels of the image. Spectra have been vertically shifted for clarity. (e) Comparison of the average I_D/I_G ratio in the central and edge regions of the flake.

curves was used to calculate the I_D/I_G ratio plotted in Fig. 2(e). A significant variation in the I_D/I_G ratio is observed in the edge region of the graphitic flake, as shown in Fig. 2(e), indicating a non-uniform distribution of disorder. To compare the level of disorder in the central and edge regions of the flake, average I_D/I_G ratios are plotted in Fig. 2(f). Although a higher average I_D/I_G ratio is observed in the central region of the flake, the large variation of the I_D/I_G ratio in the edge region suggests that the level of disorder in that region of the flakes is not significantly different from that at the center. This is further confirmed by the analysis of the I_D/I_G ratio image in Fig. S2, where a similar level of disorder is observed across the flake. Similar results were obtained in the TERS measurements of an additional unfunctionalized graphitic flake presented in Fig. S3. These results therefore indicate that there is significant disorder already present in the basal plane of the graphitic flakes, before any functionalization process is performed.

We next investigated the capability of TERS to distinguish between different degrees of functionalization. We performed TERS imaging on graphitic flakes with "low," "medium," and "high" levels of nitrogen functionalization, which will be referred to as "N_L," "N_M," and "N_H," respectively. TERS measurements of the functionalized samples were analyzed in a similar manner to those of the unfunctionalized samples and are presented in Figs. 3-5 and S3-S6. In the N_L samples (Figs. 3 and S4), a clear D peak was observed in all TERS spectra indicating disorder in the lattice. However, the I_D/I_G ratio was <0.5 [Figs. 3(d) and S4(d)], similar to the unfunctionalized samples, indicating that the level of disorder is relatively unchanged. A comparison of the I_D/I_G ratio at different locations of the flakes revealed a significant variation in the level of disorder at the edge of the flakes [Figs. 3(e) and S4(e)].

TERS measurements of N_M graphitic flakes are presented in Figs. 4 and S5. The intensity of the D and G peaks in the TERS spectra [Figs. 4(d) and S5(d)] is similar, with an I_D/I_G ratio close to 1. The higher I_D/I_G ratio observed in the N_M flakes [Figs. 4(e) and S5(e)] compared to the previous samples indicates a higher degree of disorder in the carbon lattice, due to either increased structural disorder or increased chemical functionalization. Only a slight difference in the average I_D/I_G ratio was observed in the central and edge regions of the flakes, which was within the standard deviation of the measurements signifying a relatively uniform modification of the flake with the functionalization process.

TERS imaging results of the N_H graphitic flakes are presented in Figs. 5 and S6. In the TERS images and spectra of these samples, the intensity of the D peak was significantly higher than that of the G peak [Figs. 5(b)-5(d) and S6(b)-S6(d)] with an I_D/I_G ratio > 1.3. Furthermore, compared to the N_L and N_M flakes, a significantly higher average I_D/I_G ratio was observed in the N_H flakes correlating with the increasing degree of functionalization [Figs. 5(e) and S6(e)].

A comparison of the level of disorder (I_D/I_G) for individual functionalized and unfunctionalized flakes measured using TERS and confocal Raman imaging is shown in Figs. 6(a) and 6(b), respectively. Although confocal Raman measurements cannot show the nanoscale variation across the flakes, they concur with the TERS results, Fig. 6(a), showing a clear increase in the average I_D/I_G ratio with the increasing level of functionalization in the graphitic flakes. Interestingly, a similar average I_D/I_G ratio is observed in the unfunctionalized and N_L flakes in the TERS measurements; however, this may be due to the smaller number of flakes measured with TERS compared to the confocal Raman measurements. Nonetheless, the relationship between these more in-depth but time-consuming TERS measurements and the more rapid confocal Raman spectroscopy measurements is important to provide an improved understanding of possible quality control techniques. Furthermore, TERS

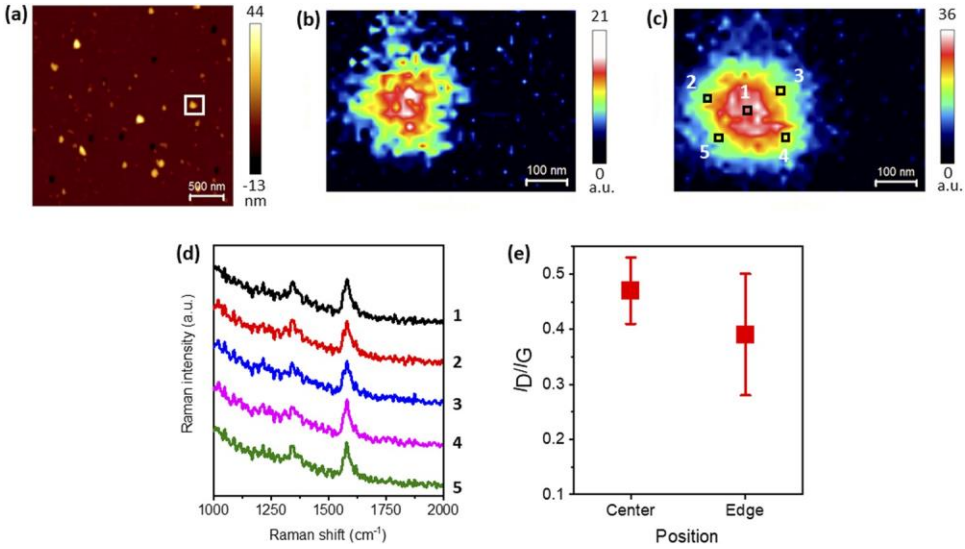

FIG. 3. (a) AFM topography image of flakes from the N_L sample. TERS images of the (b) D peak and (c) G peak intensities of the graphitic flake marked in (a). Integration time: 1 s. Step size: 15 nm. (d) Plot of average TERS spectra from the central and edge regions of the flake marked in (b). Each spectrum represents an average of four adjacent spectra. Spectra have been vertically shifted for clarity. (e) Comparison of the average I_D/I_G ratio in the central and edge regions of the flake.

measurements revealed a similar level of disorder in the central and edge regions of the functionalized samples, as shown in Fig. S7. Assuming this increased disorder is associated with the attachment of functional groups due to the functionalization process, as TERS is not able to directly detect the chemical species present here, it indicates the functional groups are not confined to the edge of the flakes only.

To confirm the hypothesis of the addition of functional groups to the graphitic material as indicated via nanoscale TERS measurements, XPS and ToF-SIMS characterization was performed on pressed pellets of the functionalized materials to confirm the change in chemistry related to the functional groups. XPS survey spectra and core level C 1s, N 1s, and O 1s spectra of the unfunctionalized and functionalized materials are presented in Fig. S8, and the calculated atomic percentage (at. %) of nitrogen and carbon measured from the samples is plotted in Fig. 6(c). The complete elemental atomic composition of the samples is listed in Table S1. An increasing trend in the at. % of nitrogen is observed with increasing functionalization, with the level of oxygen remaining roughly the same at ~4 at. %. The C 1s spectra in Fig. S8(b), shown normalized to the maximum intensity to aid the observation of differences between the samples, show an increase in the high binding energy shoulder at ~286 eV, which

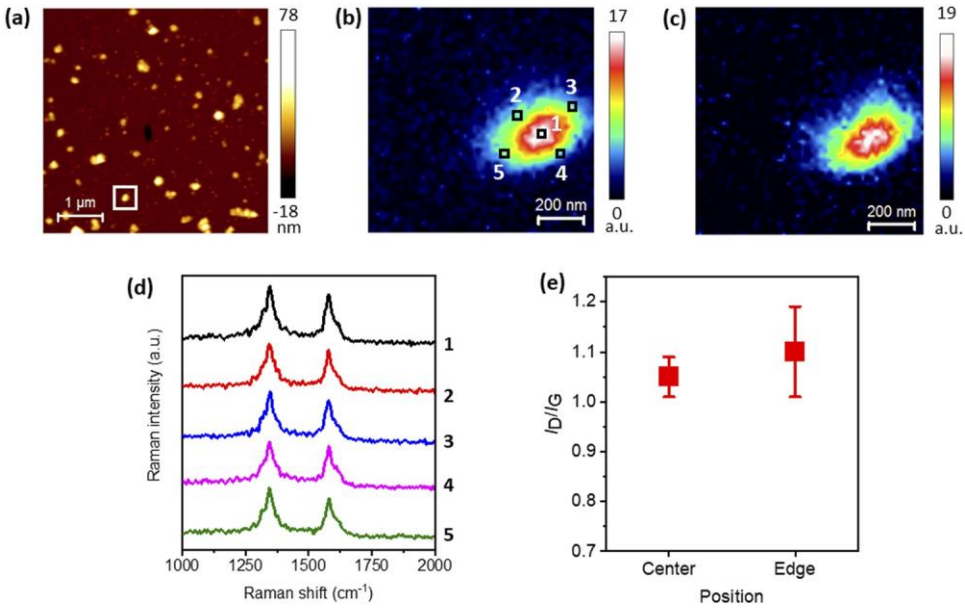

FIG. 4. (a) AFM topography image of the N_M graphitic sample. TERS images of the (b) D peak and (c) G peak intensities of the graphitic flake marked in (a). Integration time: 1 s. Step size: 20 nm. (d) Plot of average TERS spectra measured in the central and edge regions of the flake marked in (b). Each spectrum represents an average of four spectra from adjacent pixels of the image. Spectra have been vertically shifted for clarity. (e) Comparison of the average I_D/I_G ratio in the central and edge regions of the flake.

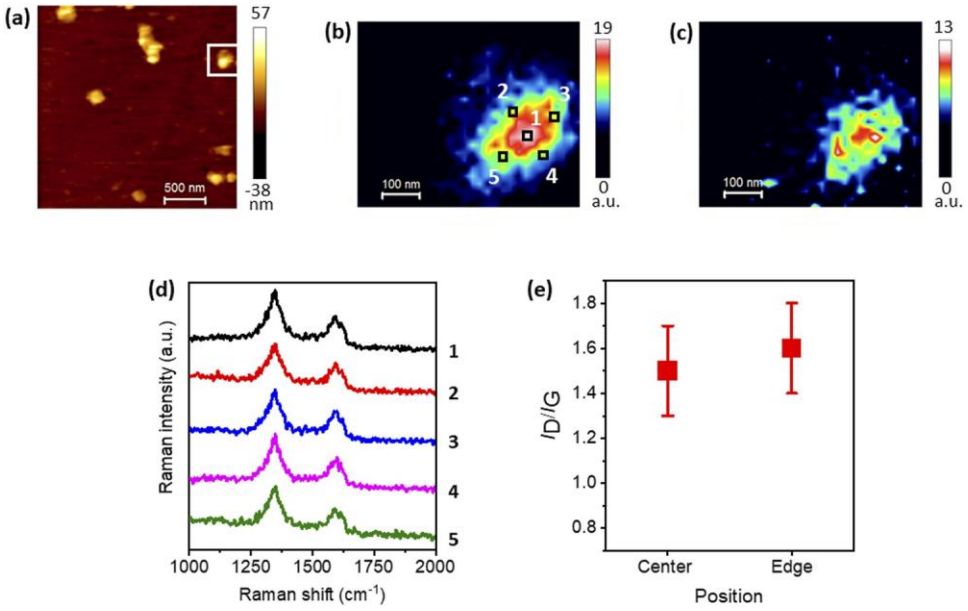

FIG. 5. (a) AFM topography image of flakes from the N_H sample. TERS images of the (b) D peak and (c) G peak intensities of the graphitic flake marked in (a). Integration time: 1 s. Step size: 20 nm. (d) Plot of average TERS spectra measured in the central and edge regions of the flake marked in (b). Each spectrum represents an average of four spectra from adjacent pixels of the image. Spectra have been vertically shifted for clarity. (e) Comparison of the average I_D/I_G ratio in the central and edge regions of the flake.

is consistent with the expected peak position of the carbon atom in a C-N bond. Again, considering the concentration of oxygen did not change with functionalization, it is reasonable to conclude that this change is due to the attachment of nitrogen containing species during functionalization.

The increase in the XPS concentration of nitrogen correlates well with the change in the I_D/I_G ratio from the TERS and confocal Raman measurements [Figs. 6(a) and 6(b)], indicating that the measured disorder is related to the increasing attachment of functional groups. This demonstrates that TERS has the sensitivity to accurately

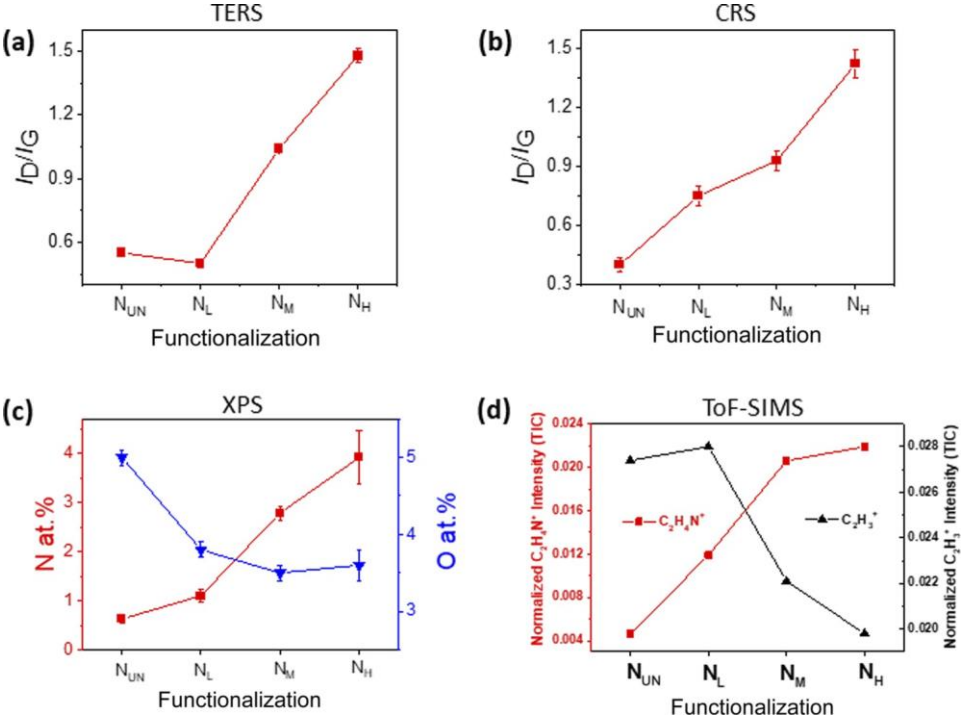

FIG. 6. Comparison of the I_D/I_G ratio from (a) TERS and (b) confocal Raman spectroscopy (CRS) measurements of the unfunctionalized (N_{UN}), N_L, N_M, and N_H samples. Each data point in (a) represents the average I_D/I_G ratio in the TERS images of the flakes shown in Figs. 2-5 and S3-S6, whereas each data point in (b) represents the average I_D/I_G ratio in the confocal Raman images of 20 graphitic flakes of each sample. (c) Plots showing at. % of nitrogen and oxygen in the graphitic samples measured using XPS. (d) Plots of secondary ion intensity, normalized to the total ion count, from positive ion spectra for $C_2H_4N^+$ (representative of nitrogen functionalization) and C_2H_{3+} (representative of the graphitic material) ions in the samples measured using ToF-SIMS.

infer differences in the level of functionalization between samples as well as where functionalization takes place on these industrially relevant graphitic materials. However, as the XPS measurements are performed on the powder in the form of a pressed pellet, the quantitative XPS assessment of the nitrogen content cannot be directly compared with the TERS images of individual particles.

Further characterization of the nitrogen containing species in the functionalized graphitic samples was performed using ToF-SIMS measurements. A representative ToF-SIMS spectrum of the unfunctionalized sample is presented in Fig. S9(a) showing different carbon and nitrogen containing species in the sample. Figure S9(b) shows 500 × 500 μm^2 ToF-SIMS images of the NO_3^-, CNO, and CN^- ion intensity in the unfunctionalized and functionalized materials measured in the center of the same pressed pellet used for the XPS measurements. An increasing trend is observed in the ion signal of these nitrogen containing species with increasing functionalization with uniform distribution over the measured area. To visualize this more clearly, the normalized intensity (with respect to the total ion count during measurements) of the CN^- negative ion peaks as well as the $C_2H_4N^+$ positive ion peaks from the total measured areas is plotted in Fig. 6(d), together with the signal from the C_2H_{3+} ion peak, which is representative of the graphitic content in the materials. An increasing trend of $C_2H_4N^+$ intensity and a decreasing trend of C_2H_{3+} intensity with increasing functionalization correlate with the TERS, confocal Raman spectroscopy, and XPS results in Figs. 6(a)-6(c), respectively. Similar trends were observed for other ion peaks such as CNO^-, NO_3^-, CH_2N^+, and CH_2NO^+, suggesting there is possibly some interaction with the residual oxygen groups of the graphitic material during functionalization. The decrease in the C_2H_{3+} ion signal indicates that a higher disorder is induced in the carbon lattice due to the attachment of functional groups across the surface of the flakes, resulting in a decreased signal from pristine graphitic regions of the flakes.

III. CONCLUSIONS

In this work, we have demonstrated the capability of TERS to spatially resolve disorder in commercially available graphitic nanomaterials induced through the presence of functional groups and compare the degree of disorder through correlation with more robust chemical characterization methods. TERS imaging was performed on graphitic samples without any chemical functionalization and with three different levels of functionalization. TERS results showed a clear increasing trend in the level of disorder determined via the I_D/I_G ratio with increasing functionalization. Furthermore, TERS measurements of disorder were correlated with the trend of increased nitrogen atomic concentration measured using XPS and the detection of nitrogen and oxygen containing ion peaks, such as $C_2H_4N^+$, CN^-, NO_3^-, and CNO^-, in ToF-SIMS measurements. Importantly, nanoscale-resolution TERS measurements facilitated spatially resolved visualization of the location of the disorder induced in the functionalized graphitic flakes revealing a similar level of functionalization in the basal plane and edge regions of the flakes. Furthermore, the TERS results were found to be in agreement with the micro-scale measurements of confocal Raman spectroscopy, which can give more rapid results, thus providing an understanding for industry of how the results from more rapid techniques are affected for materials with nanoscale characteristics. This demonstrates that a combination of spatially resolved TERS imaging with complementary chemical characterization tools such as XPS and ToF-SIMS is a powerful approach to understand the nature of nanoscale chemical functionalization in graphitic materials of direct industrial relevance.

IV. METHODS

A. Functionalization process

Commercially available few-layer graphene was placed in a patented reactor barrel and loaded into a HDPlas® plasma reactor. High nitrogen-content feed gas was fed into a low-pressure chamber where it was energized and ionized to create a plasma. Gas flow and pressure were regulated by a mass flow controller and a metered vacuum source. The reactor barrel both acted as a counter-electrode and rotated around the central electrode to facilitate mixing.

The reaction process integrates pre-treatment and post-treatment to ensure homogeneity of the starting material and product.

For production of N_L, N_M, and N_H, the material processing intensity was incrementally increased to improve reaction rates and give higher levels of nitrogen functional groups, covalently bonded to the particle surface. These materials and their associated processing details have an internal reference number of 12 653, 12 654, and 12676 for N_L, N_M, and N_H, respectively, with an internal reference number of 12 396 for the unfunctionalized material (N_{UN}).

B. Sample preparation for TERS measurements

To prepare unfunctionalized samples for TERS measurements, the as-received powder material was first dispersed in dimethylsulfoxide, with roughly 0.05 mg/ml concentration, and sonicated for 5 min in an ultrasonic bath at a frequency of 37 kHz and 80 W ultrasonic power (CamSonix C275T, Camlab, Cambridge, UK) to break any agglomerates/aggregates and obtain primary particles. The dispersion (10 µl) was then drop-cast on to a glass coverslip preheated at the boiling temperature of the solvent. To prepare functionalized samples, as-received powder materials were dispersed in N-methyl-pyrrolidone in a similar manner to unfunctionalized samples; however, their analysis showed the presence of larger particles and no isolated flakes. Therefore, functionalized samples were centrifuged at 5000 rpm (relative centrifugal force: 2655) for 60 min, and the supernatant was collected, in order to eliminate larger agglomerates/aggregates. The dispersion (10 µl) was then drop-cast on a silicon substrate or glass coverslip at the boiling temperature of the solvent. After deposition, the samples were assessed using optical microscopy (Olympus, Japan) and scanning electron microscopy (Zeiss, Germany) to select the most suitable samples containing isolated flakes for subsequent TERS measurements. Note that for SEM experiments, the substrate used was a silicon wafer with native oxide.

C. Sample preparation for XPS and ToF-SIMS measurements

Graphitic powders were pressed into pellets for XPS and ToF-SIMS analyses. Powders were pressed in a hydraulic press

(Specac, Orpington, UK) with a force of 1 ton-2 ton applied onto a 7 mm diameter die. Pellets were positioned inside an aluminum holder and fixed to the holder using carbon and copper tape for electrical conductivity.

D. TERS measurements

TERS was performed in the transmission mode on a bespoke system consisting of an inverted microscope (Nikon, Japan) fitted with an atomic force microscope (AIST-NT/Horiba Scientific, USA) on top and a Raman spectrometer (Horiba Scientific, France, grating: 600 lines/mm, focal length: 320 mm) attached to a charge coupled device detector (Andor, Ireland). A radially polarized 532 nm laser was focused onto the sample using a 100× 1.49 NA oil immersion objective lens (Nikon, Japan). TERS measurements were carried out with a laser power of 100 μW-150 μW at the sample, whereas a laser power of 650 μW was used for the confocal Raman measurements. TERS imaging was performed with a step size of 6.4 nm-23 nm.

E. XPS measurements

Chemical analysis of surface species and elemental composition was performed using an XPS instrument (Kratos Axis Ultra DLD, Kratos Analytical, Manchester, UK) with a monochromatic Al Kα x-ray source (15 kV anode potential and 5 mA emission current). The instrument was used in the "hybrid" lens mode with the "slot" entrance slit, resulting in an analysis spot of 300 × 700 μm^2 on the sample. Survey spectra were collected between 1350 eV and −10 eV with 160 eV pass energy, 1 eV step size, 0.2 ms dwell time, and two sweeps. Narrow scans were acquired for the C 1s, N 1s, and O 1s core levels with 20 eV pass energy, 100 meV step size, 500 ms dwell time, and three sweeps. Spectra were collected from three different locations within the same sample. Spectra were then analyzed with CasaXPS (Version 2.3.16) after performing a transmission function correction. The elemental composition was quantified by employing the average matrix relative sensitivity factors (AMRSFs) published by the National Physical Laboratory (NPL).[45] A Tougaard type background was employed for the analysis of all spectra.

F. ToF-SIMS measurements

ToF-SIMS measurements of the powder pellets were performed with a ToF-SIMS IV spectrometer (IONTOF GmbH, Germany), equipped with an argon gas cluster ion beam gun and a liquid metal ion gun (LMIG) oriented at 45° to the sample surface. The LMIG utilized a Bi_{3+} ion source, operating at an ion current of 0.1 pA with a beam diameter of ~2 μm, and raster-scanned randomly in the defined region of interest to be imaged on the sample. For pressed pellets of the powders, images were typically acquired over an area of 500 × 500 μm^2 with a cycle time of 100 μs, 30 scans per image, and a pixel density of 256 × 256 pixels. Spectra were measured from at least two areas of each sample. No charge compensation was needed due to the conductive nature of the pellets. The same pellets were used for both XPS and ToF-SIMS to ensure consistency of results. XPS measurements were carried out first to prevent any ion beam induced disorder from the ToF-SIMS measurements from influencing the results. All spectra were normalized to the total ion intensity to aid in the inter-sample comparison.

SUPPLEMENTARY MATERIAL

See the supplementary material for details on nanoscale resolution of TERS imaging, TERS images of additional N_{UN}, N_L, N_M, and N_H particles, a comparison of the average I_D/I_G ratio for the edge and central regions of particles from the four different materials, XPS spectra and quantitative chemical analysis, and ToF-SIMS spectra and images.

ACKNOWLEDGMENTS

This work was supported by the Analysis for Innovators (A4I) program of Innovate UK (Grant No. 121883) and the National Measurement System of the UK Department of Business, Energy and Industrial Strategy (BEIS) (Grant No. 122418). The authors would also like to thank Keith Paton from the National Physical Laboratory, UK, for useful discussions related to this work.

DATA AVAILABILITY

The data that support the findings of this study are available from the corresponding author upon reasonable request.

REFERENCES

[1]J. R. Potts, D. R. Dreyer, C. W. Bielawski, and R. S. Ruoff, Polymer **52**, 5 (2011).
[2]Q. Wu, Y. Xu, Z. Yao, A. Liu, and G. Shi, ACS Nano **4**, 1963 (2010).
[3]X. Ma, H. Tao, K. Yang, L. Feng, L. Cheng, X. Shi, Y. Li, L. Guo, and Z. Liu, Nano Res. **5**, 199 (2012).
[4]X.-D. Zhuang, Y. Chen, G. Liu, P.-P. Li, C.-X. Zhu, E.-T. Kang, K.-G. Noeh, B. Zhang, J.-H. Zhu, and Y.-X. Li, Adv. Mater. **22**, 1731 (2010).
[5]J. D. Roy-Mayhew, D. J. Bozym, C. Punckt, and I. A. Aksay, ACS Nano **4**, 6203 (2010).
[6]Y. Huang, X. Dong, Y. Liu, L.-J. Li, and P. Chen, J. Mater. Chem. **21**, 12358 (2011).
[7]V. K. Thakur and M. K. Thakur, Chemical Functionalization of Carbon Nanomaterials: Chemistry and Applications (CRC Press, 2015).
[8]V. Georgakilas, M. Otyepka, A. B. Bourlinos, V. Chandra, N. Kim, K. C. Kemp, P. Hobza, R. Zboril, and K. S. Kim, Chem. Rev. **112**, 6156 (2012).
[9]T. Kuila, S. Bose, A. K. Mishra, P. Khanra, N. H. Kim, and J. H. Lee, Prog. Mater. Sci. **57**, 1061 (2012).
[10] T. Deckert-Gaudig, A. Taguchi, S. Kawata, and V. Deckert, Chem. Soc. Rev. **46**, 4077 (2017).
[11] N. Kumar, B. M. Weckhuysen, A. J. Wain, and A. J. Pollard, Nat. Protoc. **14**, 1169 (2019).
[12] P. Verma, Chem. Rev. **117**, 6447 (2017).
[13] X. Wang, S.-C. Huang, T.-X. Huang, H.-S. Su, J.-H. Zhong, Z.-C. Zeng, M.-H. Li, and B. Ren, Chem. Soc. Rev. **46**, 4020 (2017).
[14] Y.-P. Huang, S.-C. Huang, X.-J. Wang, N. Bodappa, C.-Y. Li, H. Yin, H.-S. Su, M. Meng, H. Zhang, B. Ren, Z.-L. Yang, R. Zenobi, Z.-Q. Tian, and J.-F. Li, Angew. Chem., Int. Ed. **57**, 7523 (2018).
[15] D. Kurouski, A. Dazzi, R. Zenobi, and A. Centrone, Chem. Soc. Rev. **49**, 3315 (2020).
[16] N. Kumar, B. Stephanidis, R. Zenobi, A. J. Wain, and D. Roy, Nanoscale **7**, 7133 (2015).

[17] N. Kumar, C. S. Wondergem, A. J. Wain, and B. M. Weckhuysen, J. Phys. Chem. Lett. **10**, 1669 (2019).
[18] N. Kumar, S. Kalirai, A. J. Wain, and B. M. Weckhuysen, ChemCatChem **11**, 417 (2019).
[19] N. Kumar, A. Zoladek-Lemanczyk, A. A. Y. Guilbert, W. Su, S. M. Tuladhar, T. Kirchartz, B. C. Schroeder, I. McCulloch, J. Nelson, D. Roy, and A. Castro, Nanoscale **9**, 2723 (2017).
[20] X. Wang, D. Zhang, K. Braun, H.-J. Egelhaaf, C. J. Brabec, and A. J. Meixner, Adv. Funct. Mater. **20**, 492 (2010).
[21] N. Kumar, M. M. Drozdz, H. Jiang, D. M. Santos, and D. J. Vaux, Chem. Commun. **53**, 2451 (2017).
[22] N. Kumar, Amino Acids, Peptides and Proteins (The Royal Society of Chemistry, 2019), Vol. 43, p. 127.
[23] N. Kumar, W. Su, M. Veselý, B. M. Weckhuysen, A. J. Pollard, and A. J. Wain, Nanoscale **10**, 1815 (2018).
[24] T.-A. Yano, T. Ichimura, S. Kuwahara, F. H'Dhili, K. Uetsuki, Y. Okuno, P. Verma, and S. Kawata, Nat. Commun. **4**, 2592 (2013).
[25] Y. Okuno, Y. Saito, S. Kawata, and P. Verma, Phys. Rev. Lett. **111**, 216101 (2013).
[26] A. Weber-Bargioni, A. Schwartzberg, M. Cornaglia, A. Ismach, J. J. Urban, Y. Pang, R. Gordon, J. Bokor, M. B. Salmeron, D. F. Ogletree, P. Ashby, S. Cabrini, and P. J. Schuck, Nano Lett. **11**, 1201 (2011).
[27] M. Fleischer, A. Weber-Bargioni, M. V. P. Altoe, A. M. Schwartzberg, P. J. Schuck, S. Cabrini, and D. P. Kern, ACS Nano **5**, 2570 (2011).
[28] W. Su, N. Kumar, N. Dai, and D. Roy, Chem. Commun. **52**, 8227 (2016).
[29] W. Su, N. Kumar, A. Krayev, and M. Chaigneau, Nat. Commun. **9**, 2891 (2018).
[30] S. Mignuzzi, N. Kumar, B. Brennan, I. S. Gilmore, D. Richards, A. J. Pollard, and D. Roy, Nanoscale **7**, 19413 (2015).
[31] E. J. Legge, K. R. Paton, M. Wywijas, G. McMahon, R. Pemberton, N. Kumar, A. P. Aranga Raju, C. P. Dawson, A. J. Strudwick, J. W. Bradley, V. Stolojan, S. R. P. Silva, S. A. Hodge, B. Brennan, and A. J. Pollard, ACS Appl. Mater. Interfaces **12**, 13481 (2020).
[32] J. Rogalski, K. Braun, A. Horneber, M. van den Berg, J. Uihlein, H. Peisert, T. Chassé, A. J. Meixner, and D. Zhang, Vib. Spectrosc. **91**, 128 (2017).
[33] N. Kumar, S. Mignuzzi, W. Su, and D. Roy, EPJ Tech. Instrum. **2**, 9 (2015).
[34] W. Su, N. Kumar, S. Mignuzzi, J. Crain, and D. Roy, Nanoscale **8**, 10564 (2016).
[35] W. Su, N. Kumar, S. J. Spencer, N. Dai, and D. Roy, Nano Res. **8**, 3878 (2015).
[36] C. Casiraghi, A. Hartschuh, H. Qian, S. Piscanec, C. Georgi, A. Fasoli, K. S. Novoselov, D. M. Basko, and A. C. Ferrari, Nano Lett. **9**, 1433 (2009).
[37] M. A. Pimenta, G. Dresselhaus, M. S. Dresselhaus, L. G. Cançado, A. Jorio, and R. Saito, Phys. Chem. Chem. Phys. **9**, 1276 (2007).
[38] A. C. Ferrari, J. C. Meyer, V. Scardaci, C. Casiraghi, M. Lazzeri, F. Mauri, S. Piscanec, D. Jiang, K. S. Novoselov, S. Roth, and A. K. Geim, Phys. Rev. Lett. **97**, 187401 (2006).
[39] L. M. Malard, M. A. Pimenta, G. Dresselhaus, and M. S. Dresselhaus, Phys. Rep. **473**, 51 (2009).
[40] A. C. Ferrari and J. Robertson, Phys. Rev. B **61**, 14095 (2000).
[41] L. Gustavo Cançado, M. Gomes da Silva, E. H. Martins Ferreira, F. Hof, K. Kampioti, K. Huang, A. Pénicaud, C. Alberto Achete, R. B. Capaz, and A. Jorio, 2D Mater. **4**, 025039 (2017).
[42] A. J. Pollard, B. Brennan, H. Stec, B. J. Tyler, M. P. Seah, I. S. Gilmore, and D. Roy, Appl. Phys. Lett. **105**, 253107 (2014).
[43] A. C. Ferrari, Solid State Commun. **143**, 47 (2007).
[44] A. Eckmann, A. Felten, A. Mishchenko, L. Britnell, R. Krupke, K. S. Novoselov, and C. Casiraghi, Nano Lett. **12**, 3925 (2012).
[45] M. P. Seah, I. S. Gilmore, and S. J. Spencer, J. Electron Spectrosc. Relat. Phenom. **120**, 93 (2001).